


Research Article

Experimental Study on the Anisotropy and Non-coaxiality of Frozen Standard Sand under Different Principal Stress Directions

Dun Chen ^{1,2,3}, Guoyu Li ^{1,3}, Xiaodong Zhao ², Wei Ma ¹, Zhiwei Zhou ¹, Yanhu Mu ¹, Zejin Lai ⁴ and Tuo Chen ²

¹State Key Laboratory of Frozen Soils Engineering, Northwest Institute of Eco-environment and Resources, Chinese Academy of Sciences, Lanzhou 730000, China

²State Key Laboratory for Geomechanics and Deep Underground Engineering, China University of Mining and Technology, Xuzhou 221116, China

³Da Xing'anling Observation and Research Station of Frozen-Ground Engineering and Environment, Northwest Institute of Eco-environment and Resources, Chinese Academy of Sciences, Jiagedaqi 165000, China

⁴Gannan University of Science and Technology, Ganzhou 341000, China

Correspondence should be addressed to Guoyu Li; guoyuli@lzb.ac.cn

Received 21 February 2022; Accepted 2 April 2022; Published 14 May 2022

Academic Editor: Mohammed Fattah

Copyright © 2022 Dun Chen et al. This is an open access article distributed under the Creative Commons Attribution License, which permits unrestricted use, distribution, and reproduction in any medium, provided the original work is properly cited.

Owing to the limitations of the apparatus, the influence of its principal stress direction on the anisotropic behavior and non-coaxiality of frozen soil has not been fully considered in previous studies. At a temperature of -10°C , a series of hollow cylinder tests for frozen standard sand (FSS) was conducted under different directional angles of major principal stress and mean principal stresses in this study. The experimental results indicate that the stress-strain-strength anisotropy and non-coaxiality of the FSS are highly dependent on the principal stress direction. The stress components of the FSS vary linearly with increasing shear stress at different directional angles of the major principal stress and mean principal stresses. With a linear increase in shear stress, the strain components of the FSS exhibited a nonlinear increasing trend. The FSS strength gradually decreased as the directional angle of the major principal stress and the mean principal stresses in the test range increased. Under the different principal stress directions, the non-coaxiality of the FSS, non-coincidence of the direction of the principal strain increment and the principal stress direction, were observed. The directions of the principal strain increment and principal stress gradually tended to be coaxial as shear stress increased. Although the non-coaxial angle of the FSS increased gradually with an increase in the directional angles of the major principal stress, it did not change with the change in the mean principal stress. The non-coaxial angle of the FSS was observed to be as large as 35° in the early stage of shearing under different mean principal stresses.

1. Introduction

The principal stress direction varies in almost all geotechnical constructions [1–4],

such as earthquakes, traffic loading, and sea waves, and significantly impacts geotechnical engineering. Numerous experimental studies have been conducted to verify the anisotropic behavior and non-coaxiality of soil under different principal stress directions [3, 4]. Anisotropic behavior and non-coaxiality are two important characteristics of soil that substantially influence its mechanical behavior [5–7].

When designing infrastructure, without considering the influence of these soil characteristics, the deformation of the soil may be severely underestimated. Therefore, it is important to investigate the anisotropic behavior and non-coaxiality of frozen soil, to understand mechanical behavior under different principal stress directions.

Depending on the cause, soil anisotropy can be classified as inherent anisotropy or stress-induced anisotropy [5]. Stress-induced anisotropy refers to the difference in the mechanical properties of soil in different stress directions triggered by various stress conditions under complex stress

TABLE 1: Equations for data interpretation [39].

	Stress	Strain
Axial	$\sigma_z = (W/(\pi(r_o^2 - r_i^2))) + ((p_o(r_o^2 - r_p^2) - p_i r_i^2)/(r_o^2 - r_i^2))$	$\epsilon_z = \Delta h/H_o$
Circumferential normal	$\sigma_\theta = (p_o r_o - p_i r_i)/(r_o - r_i)$	$\epsilon_\theta = -(u_o + u_i)/(r_o + r_i)$
Radial	$\sigma_r = (p_o r_o + p_i r_i)/(r_o + r_i)$	$\epsilon_r = -(u_o - u_i)/(r_o - r_i)$
Circumferential shear	$\tau_{z\theta} = \tau_{\theta z} = (M_T(r_o + r_i))/(\pi(r_o^4 - r_i^4))$	$\gamma_{z\theta} = \gamma_{\theta z} = (2\Delta\theta(r_o^3 - r_i^3))/(3H_o(r_o^2 - r_i^2))$
Major principal	$\sigma_1 = (\sigma_z + \sigma_\theta)/2 + \sqrt{((\sigma_z - \sigma_\theta)/2)^2 + (\tau_{z\theta})^2}$	$\epsilon_1 = (\epsilon_z + \epsilon_\theta)/2 + \sqrt{((\epsilon_z - \epsilon_\theta)/2)^2 + (\gamma_{z\theta})^2}$
Intermediate principal	$\sigma_2 = \sigma_r$	$\epsilon_2 = \epsilon_r$
Minor principal	$\sigma_3 = (\sigma_z + \sigma_\theta)/2 - \sqrt{((\sigma_z - \sigma_\theta)/2)^2 + (\tau_{z\theta})^2}$	$\epsilon_3 = (\epsilon_z + \epsilon_\theta)/2 - \sqrt{((\epsilon_z - \epsilon_\theta)/2)^2 + (\gamma_{z\theta})^2}$

states. Several studies on the stress-strain-strength anisotropy of soil have been conducted from both micro and macro perspectives. Microscopic analysis has revealed the mechanism of soil properties in different stress directions from the fabric and arrangement of soil particles, whereas macroscopic analysis has elucidated the anisotropic behavior of soil through mechanical properties, such as modulus, stress-strain properties, and strength under different stress paths. Several scholars have investigated the anisotropic characteristics of soil at the microscopic level, comparing the fabric and particle arrangement of soil before and after test loading via the electrical conductivity method (ECM) [5], scanning electron microscopy (SEM) [6], computed tomography (CT) scanning, X-ray methods, and discrete element methods (DEM) [7]. Klein and Santamarina [5] identified anisotropic behavior in the structure of mica sheets using ECM tests. Ye et al. [6] conducted SEM tests on soft soil from the eastern China and discovered that permeability varied in the horizontal and vertical directions. In addition, seepage characteristics were verified to be closely related to the pore distribution and connectivity. Jiang et al. [7] investigated the macro and micro anisotropic behaviors of soil using numerical techniques, such as DEM, and then discovered that the macroscopic anisotropy of soil depends on the anisotropy of the arrangement of its microstructure. Several researchers [8–11] have investigated the anisotropic behavior of soil using different geotechnical tests in the macroscopic study of soil anisotropy and discovered that the stress loading directions significantly influence the mechanical properties of soil. Bodner [8] reported that the shear strength of clay is closely related to the shear failure surface based on an earlier study on the anisotropic behavior of soil through direct-shear tests. Gong [9] investigated the anisotropic behavior of soil in various specimen cutting directions using triaxial compression tests. This study identified a link between specimen cutting angle and soil strength. The anisotropic behavior of the soil was then obtained in experimental studies on sand using a true triaxial apparatus that can control stress in three orthogonal directions [10, 11]. The true triaxial test revealed that the deformation of sand in three different orthogonal directions exhibited clear anisotropic behavior. Despite extensive studies on the anisotropic behavior of soil, it does not correspond



FIGURE 1: China's ISO standard sand.

TABLE 2: Physical properties of standard sand.

Specific gravity G_s	Nonuniformity coefficient C_U	Curvature coefficient C_C	Particle size D	Dry density g/cm^3
2.643	1.16	1.06	0.5–1.0	1.53

to the actual stress state was triggered by the principal stress direction in the field. The hollow cylinder apparatus (HCA) was employed to determine the anisotropy of the soil while considering the influence of principal stress rotation. Symes et al. [1] published a study on the anisotropy of soil under various principal stress directions. Several researchers [12–17] have previously investigated the anisotropic behavior of sand and clay using HCA tests, and the obtained results have suggested that the strength and stress-strain response of soil strongly depend on the change in the principal stress direction. Moreover, multiple researchers [18, 19] have investigated the anisotropic behavior of soils subjected to principal stress rotation. These investigations indicate that the variations in the principal stress direction are related to the mechanical properties of the saturated soft clay.

Non-coaxiality is defined as the non-coincidence of the direction of the principal strain increment and the direction of the principal stress [20]. Non-coaxiality is the key to understanding strength behavior and establishing constitutive models of soil. Roscoe et al. [21] discovered the non-coaxiality of soil with principal stress direction inconsistent with the direction of the plastic principal strain increment

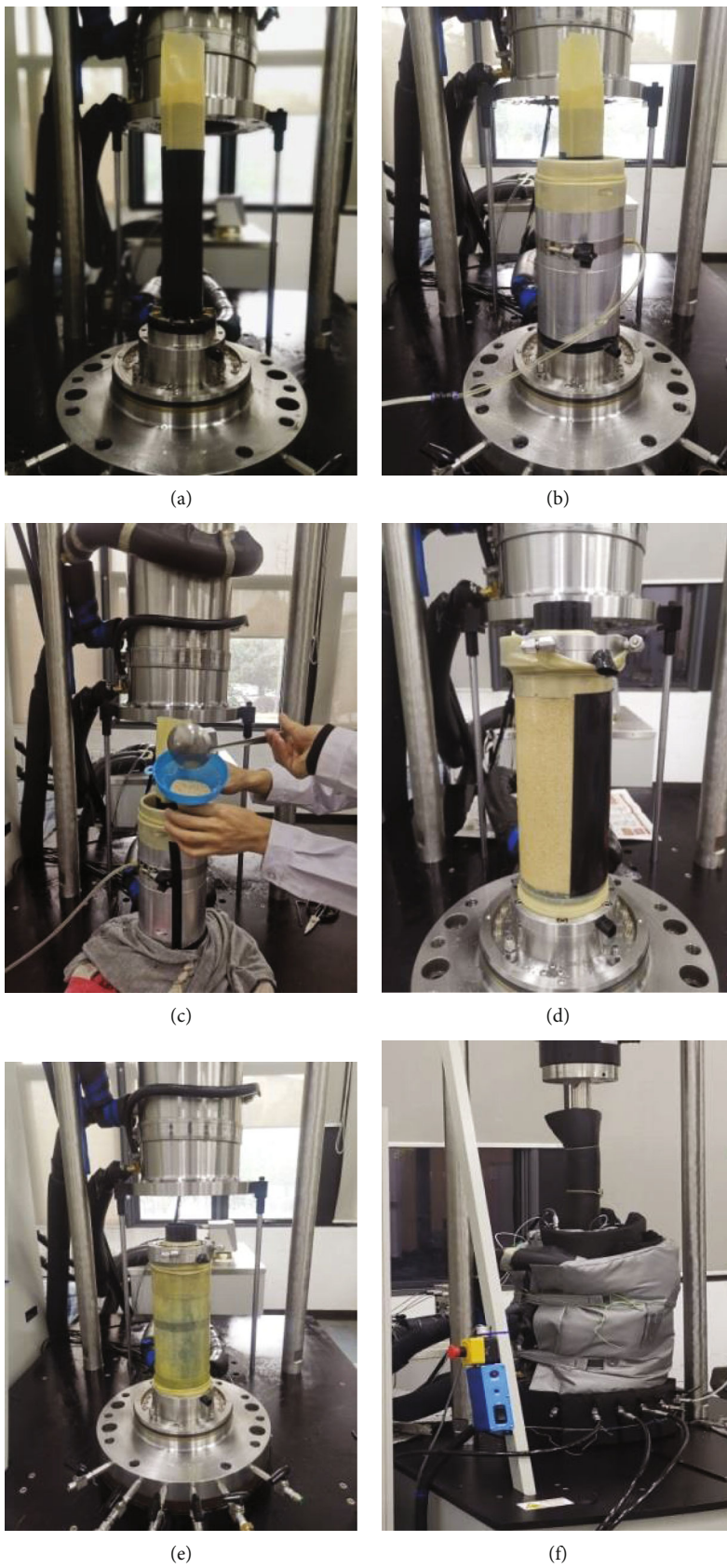


FIGURE 2: Preparation procedures of hollow cylindrical specimen of the FSS.

TABLE 3: Summary of directional shear tests.

Test Nos.	$T/(^{\circ}\text{C})$	$\alpha/(^{\circ})$	$p/(\text{MPa})$	b
T1	-10	0	4.5	0.5
T2	-10	15	4.5	0.5
T3	-10	30	4.5	0.5
T4	-10	30	2	0.5
T5	-10	30	6	0.5

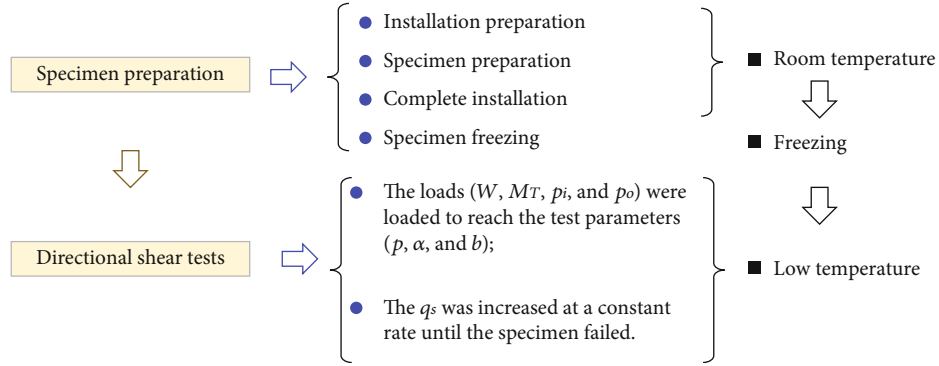


FIGURE 3: Flowchart of testing program.

as early as the 1960s using direct shear tests. The non-coaxiality of the soil was clearer at the beginning of shearing; however, as the specimen approached failure, the directions of the plastic principal strain increment and the principal stress tended to be coaxial. Wong and Arthur [22] discovered that the rotation of the principal stress axis triggers a non-coaxial behavior, with the angle between the principal stress direction and the direction of the principal strain increment reaching up to 30° . Numerous studies conducted in recent years have demonstrated the non-coaxiality of soil using HCA, owing to the advancement of test instruments. Symes et al. [1] conducted undrained tests on sand, confirmed the existence of the non-coaxiality of sand under a directional shear stress path, and discovered that the non-coaxial angle gradually decreased with an increase in shear stress, eventually tending to be coaxial. According to some researchers, the non-coaxiality of Toyoura sand is clearer under the continuous rotation of the principal stress axis than under monotonic shear [23–25]. Numerous experimental studies conducted recently have demonstrated the non-coaxial behavior of soil under directional shear stress path, with the elastic component exerting a minor influence [26–30]. However, owing to the limitations of the apparatus, the non-coaxiality characteristics of frozen soil under different principal stress directions are yet to be investigated.

As summarized above, several experimental studies on anisotropy and non-coaxiality, as represented by variations in the principal stress direction, on soil behavior have been reported in the literature. However, there have been no attempts to present the anisotropy and non-coaxial behavior of frozen soil. Several researchers have investigated the mechanical properties of frozen soil using conventional geotechnical tests [31–37]. In previous studies, HCA tests have

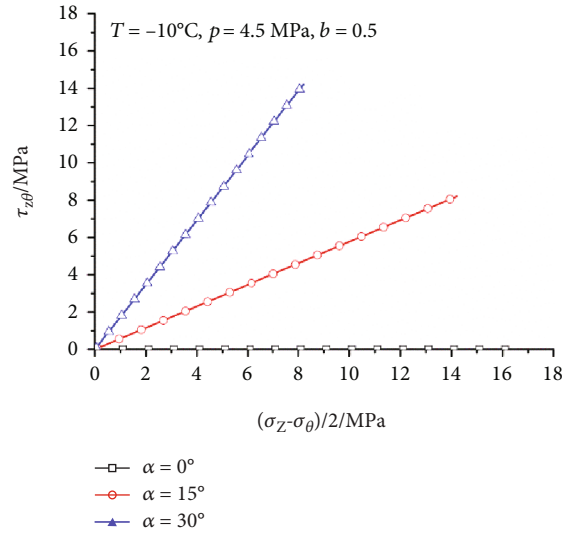


FIGURE 4: Stress path under different principal stress directions.

not been used as a preferred method for studying the anisotropic behaviors and non-coaxiality of frozen soil because they are limited by laboratory methods. Recently, although the strength and dynamic deformation of frozen clay have been described and analyzed by researchers using the dynamic hollow cylinder apparatus for frozen soil (FHCA-300) [2, 38, 39], the stress-strain-strength anisotropy and non-coaxiality of frozen soil that varies with the in situ loading direction cannot be simulated. Hence, the non-coaxiality phenomenon of frozen soil has not been studied, and research on the anisotropy of frozen soil remains insufficient. Therefore, in this study, we present an

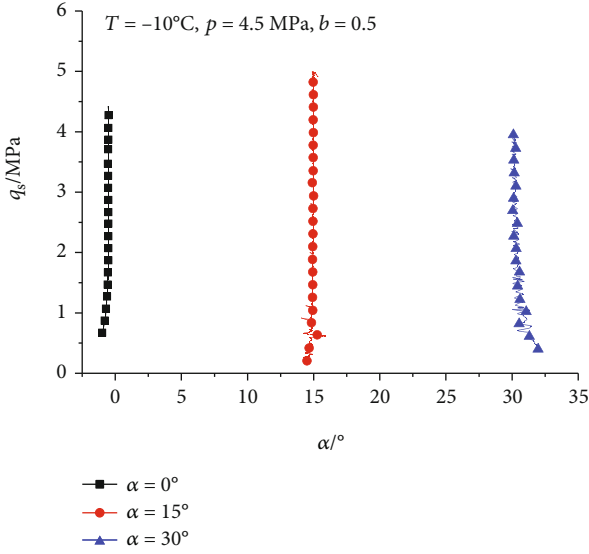


FIGURE 5: Relationships between directional angle of the major principal stress and shear stress under different principal stress directions.

experimental study on the anisotropy and non-coaxiality of frozen standard sand (FSS) using the FHCA-300, which considers the influence of the principal stress direction. The test results of directional shear stress path with different directional angles of the major principal stress and mean principal stresses on the FSS were presented and analyzed. These studies can provide further insights into the influence of principal stress direction on the mechanical characteristics of frozen soil.

2. Research Significance

Anisotropy and non-coaxiality, two important characteristics of soil, significantly impact on the mechanical behavior of soil [1, 40]. Varying strengths and stress-strain relationships of frozen soil were observed with different stress paths, particularly under different principal stress directions, exhibiting significant anisotropic characteristics of frozen soil [38, 39]. The stress-strain-strength behaviors of frozen clay are substantially affected by the fixed direction of principal stress, which has an evident anisotropic behavior of frozen clay [2, 38]. However, anisotropic behavior, especially considering the effect of the various directions of principal stress, has rarely been reported for the FSS. Therefore, the anisotropic behavior of the FSS under different principal stress directions must be investigated.

Conventional elastic-plastic constitutive models of frozen soil were used to predict the deformation and strength under different stress states. The coaxiality assumption (the consistency between the directions of the principal strain increment and principal stress) has been implied in the constitutive models of frozen soil established in the past [31–37], which cannot reflect non-coaxiality, thereby resulting in a serious underestimation of the deformation of the frozen soil. Infrastructure design that does not consider the

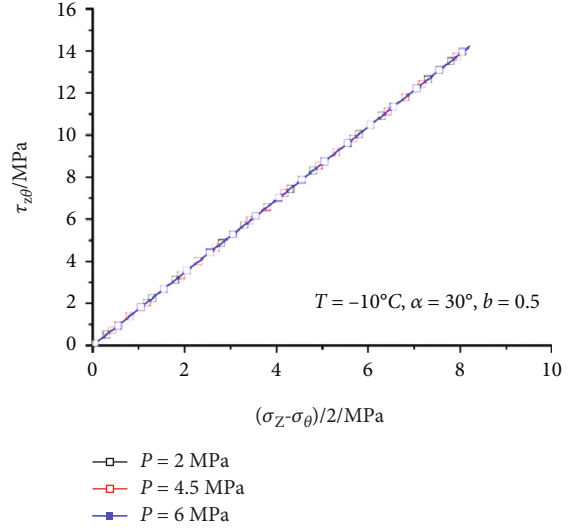


FIGURE 6: Stress path under different mean principal stresses.

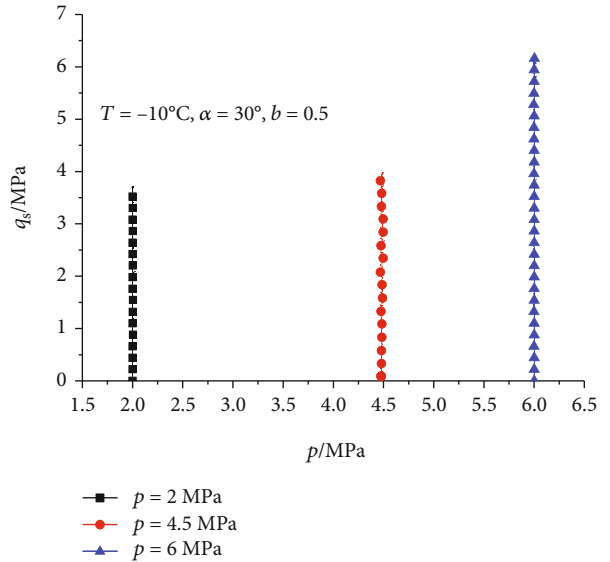


FIGURE 7: Relationships between mean principal stress and shear stress under different mean principal stresses.

effect of non-coaxiality may be unsafe in permafrost regions. The evolution law of non-coaxiality characteristics in frozen soil is unclear, especially under the stress paths involved in the principal stress direction. Therefore, it is important to consider the non-coaxiality of frozen soil in the mechanical behavior and constitutive model of frozen soil under different principal stress directions. The primary purpose of this study is to use the FHCA-300 to investigate the anisotropy and non-coaxiality of the FSS under different principal stress directions.

3. Materials and Laboratory Tests

3.1. *Test Apparatus.* The experiments in this study were performed using the FHCA-300. Chen et al. [38] provided

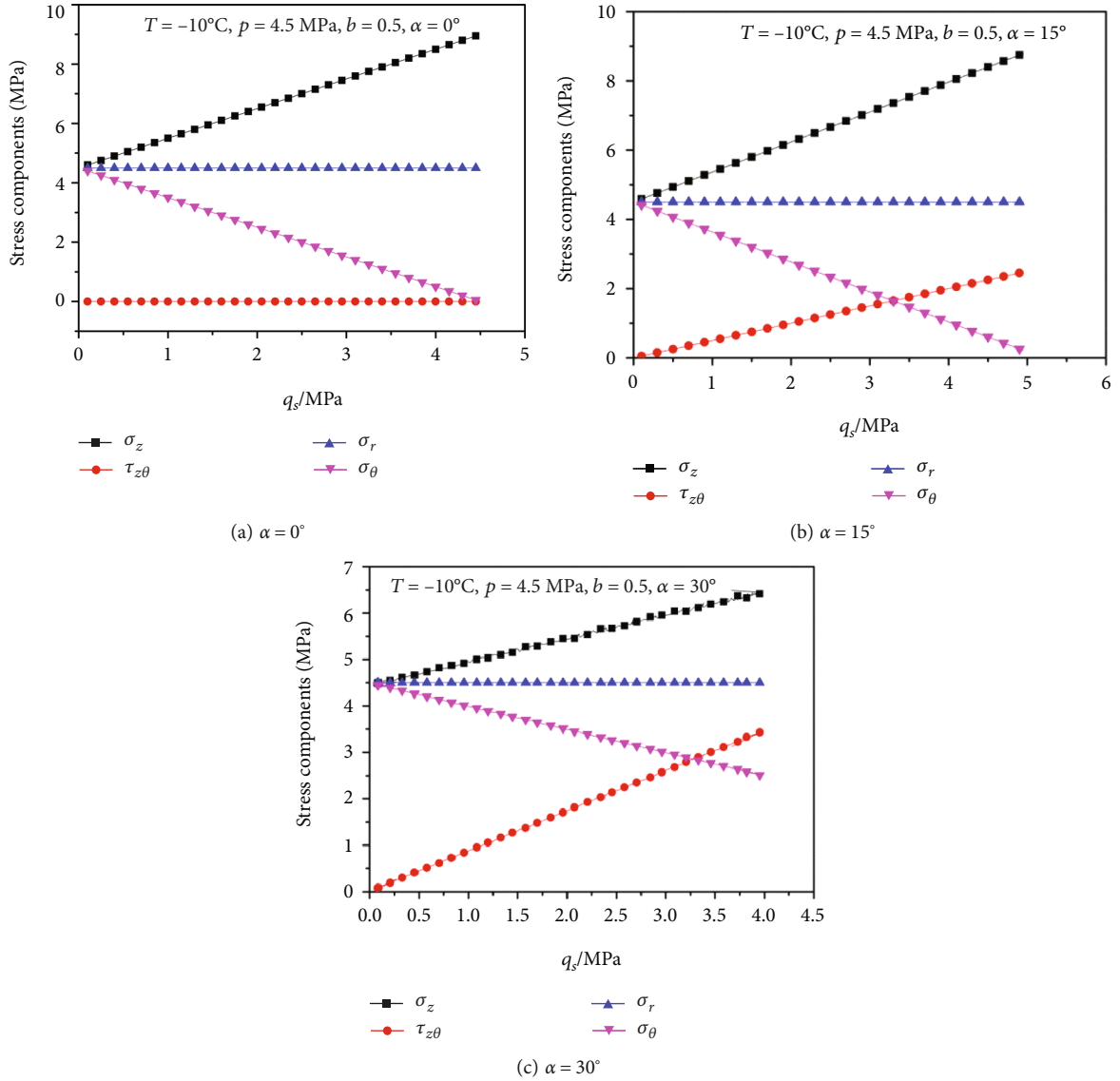


FIGURE 8: Relationships between shear stress and stress components of the FSS.

a detailed description of apparatus functions. Unlike other geotechnical test apparatus, the FHCA-300 can perform principal stress rotations at different temperatures [38, 39]. The HCA tests are extremely useful for studying the mechanical behavior of frozen soil under complex loading conditions. Therefore, complex geotechnical tests with multiple stress paths (such as directional shear stress paths) can be performed.

By applying controlled loads (W , M_T , p_i , and p_o), the four stress components (σ_z , σ_r , σ_θ , and $\tau_{z\theta}$) of the hollow cylindrical soil specimens can be controlled. Hight et al. [18] provided the equations for calculating the stress and strain components, as presented in Table 1. The non-coaxial angle is adopted to quantify the degree of non-coaxiality and is defined as the angle between the directions of the principal strain increment and principal stress [18]. The non-coaxial angle can be calculated as

$$\alpha = \frac{1}{2} \arctan \left(\frac{2\tau_{z\theta}}{\sigma_z - \sigma_\theta} \right). \quad (1)$$

$$\alpha_{ds} = \frac{1}{2} \arctan \left(\frac{d\gamma_{z\theta}}{d\varepsilon_z - d\varepsilon_\theta} \right). \quad (2)$$

$$\beta = \alpha_{ds} - \alpha. \quad (3)$$

3.2. Specimen Preparation

3.2.1. Material Selection. In a series of experiments, China's ISO standard sand was adopted to circumvent differences caused by the inherent anisotropy of frozen soil (refer to Figure 1). The specific gravity and particle size of standard sand were determined as 2.643 and 0.5–1.0 mm, respectively. Their physical properties are presented in Table 2.

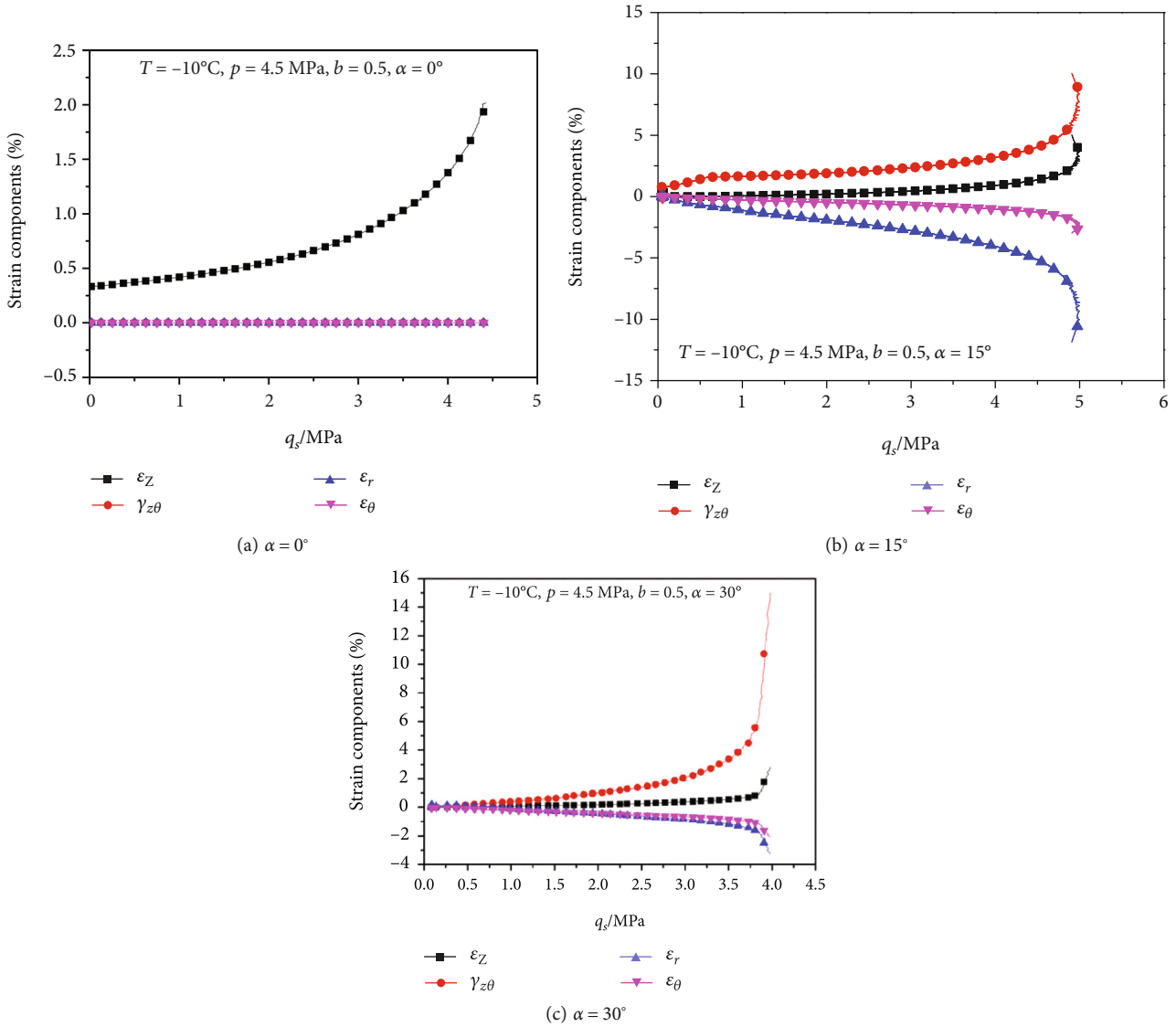


FIGURE 9: Relationships between shear stress and strain components of the FSS.

3.2.2. *Specimen Preparation Method.* Compared with the specimen preparation of frozen clay [38], the hollow cylindrical specimen of the FSS was prepared on the FHCA-300, with dimensions of 100 mm/60 mm/200 mm (OD/ID/height). In this study, the hollow cylindrical specimen of the FSS was prepared using the following procedure (as shown in Figure 2):

- (a) *Installation preparation.* The inner membrane was inserted into the bottom of the base pedestal of the FHCA-300 by the “O” shaped rubber ring, as illustrated in Figure 2(a). The outer membrane and mold (refer to Figure 2(b)) were then assembled on the base pedestal of the FHCA-300.
- (b) *Specimen preparation.* The pluviation method was adopted to create a hollow cylindrical specimen of the FSS. In addition, the prepared dry sand was sprinkled evenly along the gap between the inner

and outer membranes using a funnel (Figure 2(c)). The top surface of the hollow cylindrical specimen was leveled with a brush, and the upper indenter was installed for sealing, as illustrated in Figures 2(d) and 2(e).

- (c) *Complete installation.* First, a pressure rod was employed to fix the upper part of the specimen. Second, after slowly lowering and tightening the cell chamber of the FHCA-300, the outer and inner cells were filled with aviation oil. Third, as illustrated in Figure 2(f), the pressure tank was wrapped with thermal insulation foam to protect it from external heat exchange.
- (d) *Specimen freezing.* Under vacuum conditions, the hollow cylindrical specimens of the FSS were suctioned in distilled water until they were fully saturated. The FSS specimens were then quickly frozen

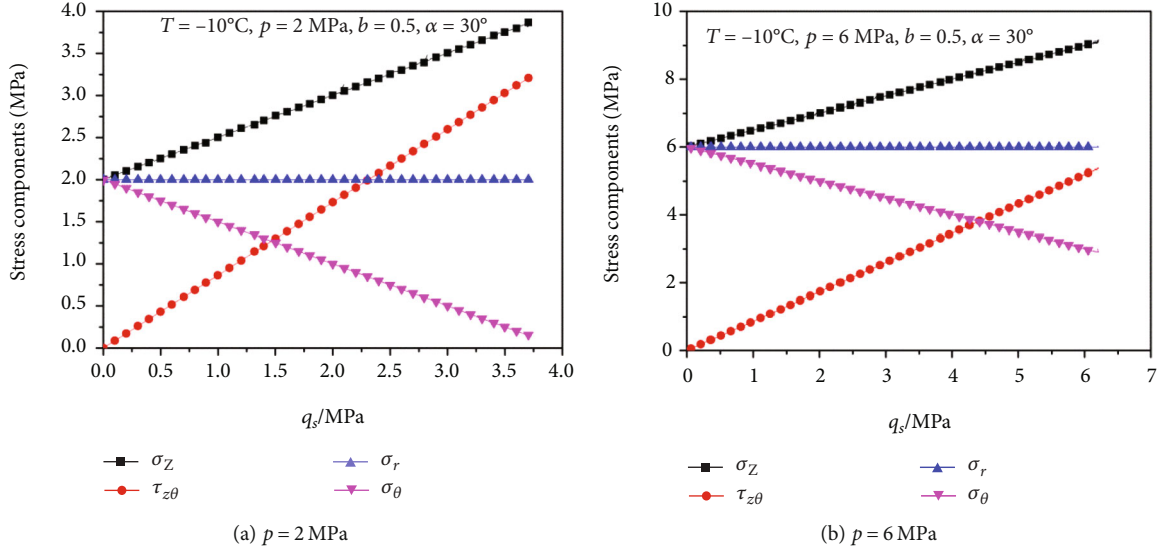


FIGURE 10: Relationships between shear stress and stress components of the FSS.

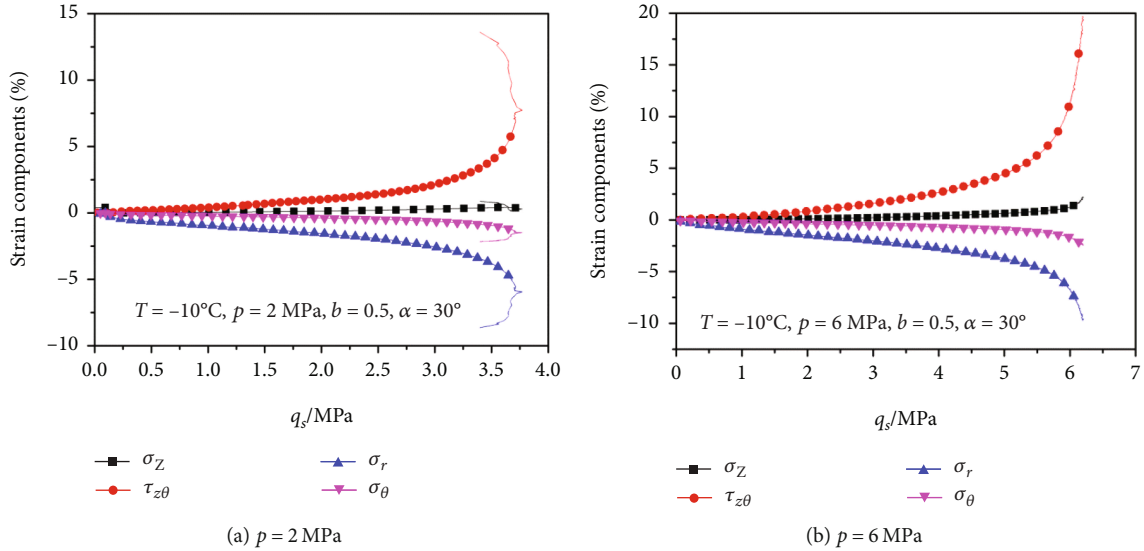


FIGURE 11: Relationships between shear stress and strain components of the FSS.

at -30°C for 48 h. The HCA tests of the FSS began after the specimen temperature was increased to -10°C and maintained for 12 h.

3.3. Program of Laboratory Tests. The stress path of directional shear was selected in this study to investigate the anisotropic behavior and non-coaxiality of the FSS under different principal stress directions. The hollow cylindrical specimens of the FSS were subjected to a series of HCA tests at $\alpha = 0^\circ, 15^\circ, \text{ and } 30^\circ$ with $p = 2, 4.5, \text{ and } 6$ MPa. Meanwhile, as illustrated in Table 3, all tests in this study were performed keeping T constant at -10°C and b at 0.5.

The four parameters (p , α , b , and T) remained constant during the stress path loading step, while q_s was increased at a rate of 30 kPa/min until σ_z reached 20% or $\gamma_{z\theta}$ reached 30% [41], i.e., the shear stress increased along the different

parameters (α and p) until failure occurred. A flowchart of the testing program is presented in Figure 3.

4. Results and Discussion

4.1. Realization of Directional Shear Stress Path. In this study, the stress path of the directional shear was followed. A series of HCA tests were performed on frozen soil at different α and p values. As illustrated in Figure 4, the stress path of the directional shear was determined by increasing q_s until failure, while the α value was fixed at $0^\circ, 15^\circ, \text{ and } 30^\circ$. The angle between $(\sigma_z - \sigma_\theta)/2$ and $\tau_{z\theta}$ was twice the directional angle of the major principal stress as given by Equation (1). In the deviatoric stress space, α value remained constant, and the hollow cylindrical specimen of the FSS was along the loading stress path until the specimen failed, as illustrated in Figure 5. The corresponding values of the mean

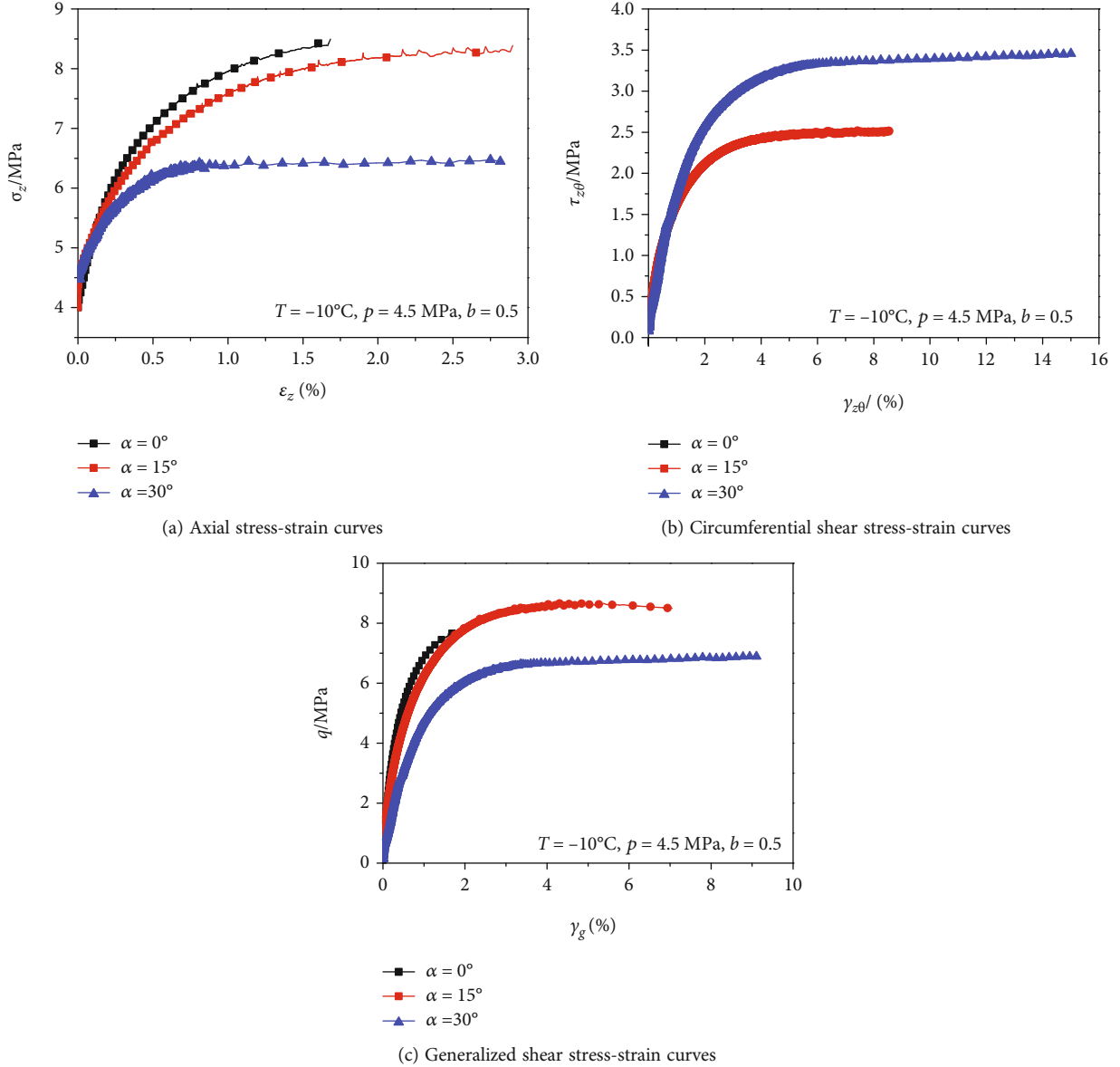


FIGURE 12: Stress-strain curves of the FSS under different principal stress directions.

principal stresses when $\alpha = 30^\circ$ are 2 MPa, 4.5 MPa, and 6 MPa (as shown in Figures 6 and 7), respectively. In Figure 6, the stress paths overlap because the directional angles of the major principal stresses are all 30° in the deviatoric stress space, thereby confirming the accuracy of the loading paths. In summary, the actual stress paths (scatter points) closely match the theoretical curves (solid lines).

4.2. Stress and Strain Component Characteristic of the FSS under the Directional Shear Stress Path. This section presents and discusses the results obtained from a series of the FSS tests with varying p and α value. Based on Table 1, the following equations can be used to calculate the corresponding relationship between the generalized stresses (q_s , p , α , and b) and stress components (σ_z , σ_r , σ_θ , and $\tau_{z\theta}$) [42]:

$$\begin{aligned}
 \sigma_z &= p - \frac{(2bq_s - q/2)}{3} + (q_s) \cos(2\alpha), \\
 \sigma_r &= p + \frac{2(2bq_s - q_s)}{3}, \\
 \sigma_\theta &= p - \frac{(2bq_s - q_s)}{3} - (q_s) \cos(2\alpha), \\
 \tau_{z\theta} &= (q_s) \sin(2\alpha).
 \end{aligned} \tag{4}$$

4.2.1. Stress Characteristics of the FSS under Different Directional Angles of Major Principal Stress. Figure 8 presents the relationships between q_s and the stress components of the FSS under different α values at $T = -10^\circ\text{C}$. The following features can be clearly identified: (a) the σ_z of the FSS increases linearly with increasing q_s under the directional

shear stress path; however, the increased amplitude of the axial stress varies with the α value; (b) when $\alpha = 0^\circ$, the hollow cylindrical specimen of the FSS is only subjected to an axial load, and $\tau_{z\theta}$ is always zero throughout the loading procedure; (c) the σ_r of the FSS is always constant with the linear increase in q_s , and the value is equal to the mean principal stress ($p = 4.5$ MPa); (d) the σ_θ of the FSS decreases with increasing q_s ; and (e) when $\alpha = 15^\circ$ and 30° , the axial stress and circumferential shear stress of the FSS increases simultaneously owing to the coupling effect of axial load and torque, and the hollow cylindrical specimen of the FSS exhibits both compression and torsional shears.

4.2.2. Strain Characteristics of the FSS under Different Directional Angles of Major Principal Stress. Figure 9 presents the variations in q_s and the strain components of the FSS under different α values. The development of the strain component curves of the FSS exhibits significant differences with the nonlinear increase in shear stress under the directional shear stress path. Only the axial strain of the FSS increases nonlinearly with an increase in q_s at $\alpha = 0^\circ$, as illustrated in Figure 9(a); $\gamma_{z\theta}$, ϵ_r , and ϵ_θ are always maintained at zero. The strain component exhibits a nonlinear growth trend at $\alpha = 15^\circ$ and 30° . And the hollow cylindrical specimen of the FSS exhibits the axial compression and radial expansion states owing to the coupling effects of the axial load and torque. Therefore, the radial strain of the FSS exhibits a negative growth trend at $\alpha = 15^\circ$ and 30° . Simultaneously, the strain components exhibit a slow growth trend in the early stage and then a rapid growth trend as they approach failure.

4.2.3. Stress Characteristics of the FSS under Different Mean Principal Stresses. The stress components are plotted against the shear stress in Figures 10(a) and 10(b) at $p = 2$ and 6 MPa, respectively. Figure 8(c) depicts the relationship curves between the stress components and shear stress with $p = 4.5$ MPa under $\alpha = 30^\circ$ at $T = -10^\circ\text{C}$. The different stress components change linearly with an increase in q_s during the directional shear tests of the FSS. As q_s , σ_z , and $\tau_{z\theta}$ increase linearly, σ_θ decreases linearly, while the σ_r simultaneously remains constant, with its value being equal to the mean principal stress.

4.2.4. Strain Characteristics of the FSS under Different Mean Principal Stresses. Figures 11(a), 9(c), and 11(b) present the strain components versus shear stress obtained from experiments under $p = 2, 4.5,$ and 6 MPa at $T = -10^\circ\text{C}$, respectively. During the shearing process, the strain component curves of the FSS exhibit a nonlinear increase with a linear increase in q_s , thus indicating that the strain component initially increases slowly and then rapidly it approached failure. The radial strain and circumferential normal strain increase negatively as q_s increases; however, the variation in the radial strain is greater than that in the circumferential normal strain of the FSS.

4.3. Anisotropy Behavior of the FSS

4.3.1. Strength Characteristics of the FSS under Different Directional Angles of Major Principal Stress. A series of FSS tests were performed using the FHCA-300 to determine

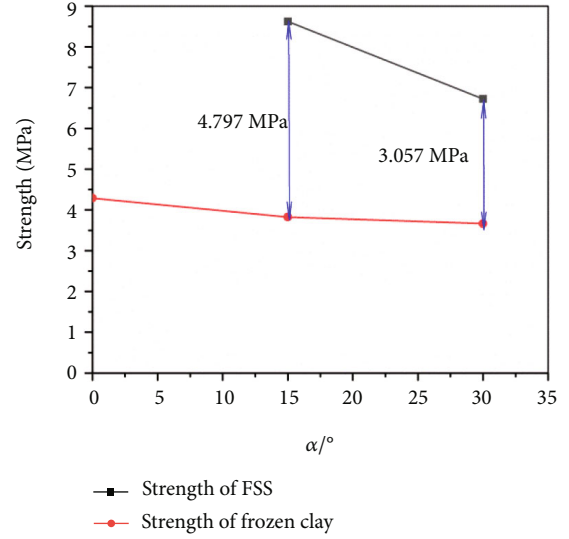


FIGURE 13: Strength variations of the FSS and frozen clay with different principal stress directions.

the effects of different principal stress directions on deformation and strength. From Figure 12, the strain components develop with stress components with $p = 4.5$ MPa under $\alpha = 0^\circ, 15^\circ,$ and 30° at $T = -10^\circ\text{C}$ and $b = 0.5$.

Figure 12(a) illustrates the relationship between the axial stress and strain of the FSS. Under different principal stress directions, the axial stress-strain curves of the FSS all exhibit the strain-hardening phenomena. The axial strength of the FSS gradually decreases as α increases. The anisotropy of the FSS was induced by the principal stress direction. Figure 12(b) depicts the circumferential shear stress-strain behavior of the FSS at various values of α . The torsional shear strength of the FSS increases with increasing α value in the directional shear tests. The principal stress direction had a significant impact on the torsional shear strength of the FSS. When $\alpha = 0^\circ$, the hollow cylindrical specimens of the FSS were only subjected to an axial load, thereby resulting in approximately zero of circumferential shear strain. However, the circumferential shear stress-strain curves exhibit strain hardening at $\alpha = 15^\circ$ and 30° . Figure 12(c) illustrates the relationship between the generalized shear stress-strain curves obtained from the directional shear tests of the FSS under different principal stress directions. The generalized shear stress-strain curves of the FSS are primarily strain-hardening curves. However, the generalized shear stress-strain curves of the FSS exhibit a weak hardening tendency at $\alpha = 15^\circ$. The strength of the FSS gradually decreases as α value increases. The axial component dominates the generalized shear stress-strain curves of the FSS more than the circumferential shear component.

In this study, the q value corresponding to $\gamma_g = 5\%$ was considered as the failure point of the FSS. Figure 13 illustrates the changes in the strength of the FSS and frozen clay at various α values. Chen et al. [38] described the test data for frozen clay with the same stress path as that of the FSS. As observed in Figure 13, the strengths of the FSS and frozen

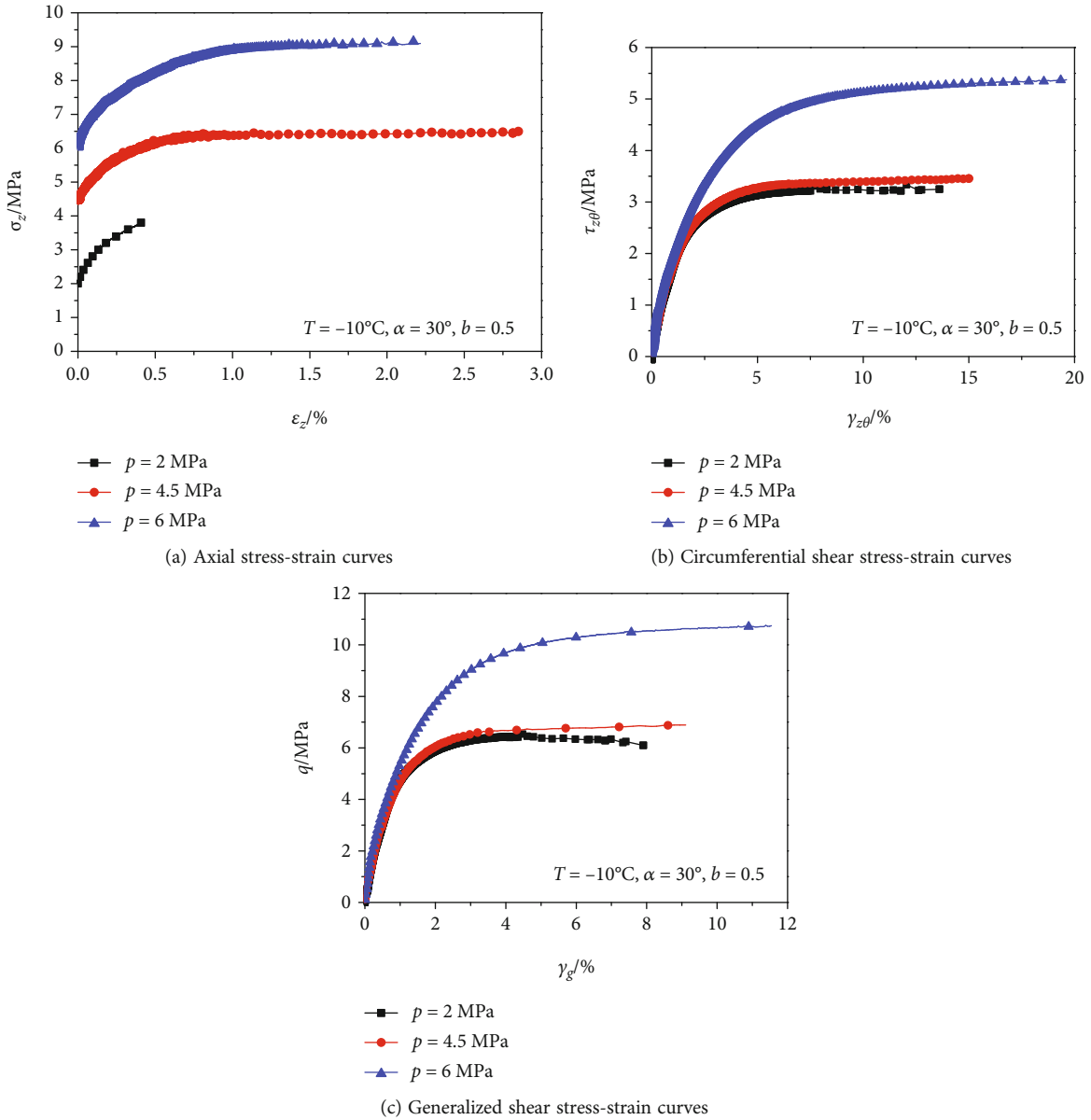


FIGURE 14: Stress-strain curves of the FSS under different mean principal stresses.

clay differ in two ways: on the one hand, the strength of the FSS is greater than that of the frozen clay under the same directional angle of major principal stress; the strength deviation between the FSS and frozen clay can be as large as 4.797 MPa and 3.057 MPa at $\alpha = 15^\circ$ and 30° , respectively; on the other hand, with the variation in α value, the strength of the FSS varies more abruptly than that of the frozen clay. Based on the preceding analysis and discussion, it can be inferred that the anisotropic behavior of frozen soil is caused by the principal stress direction; frozen soil exhibits stress-strain-strength variations depending on the principal stress directions.

4.3.2. *Strength Characteristics of the FSS under Different Mean Principal Stresses.* Figure 14 presents the variations in the FSS with stress and strain under $p = 2, 4.5,$ and 6 MPa at $T = -10^\circ\text{C}$. The axial stress-strain curves of the FSS

exhibit strain-hardening characteristics under different mean principal stresses. The strength gradually increases as the p value increases. The hollow cylindrical specimen of the FSS was always compressed. Figures 14(b) and 14(c) present the circumferential shear and generalized shear stress-strain curves of the FSS, respectively. The strength of the FSS gradually increases as the p value increases within the test range. The strength of the FSS at $p = 6$ MPa was significantly higher than those at $p = 2$ and 4.5 MPa.

4.4. *Non-coaxiality of the FSS*

4.4.1. *Non-coaxiality of the FSS under Different Directional Angles of Major Principal Stress.* The relationship between β and q_s was calculated based on the test data of the FSS under different fixed principal stress directions. Figure 15

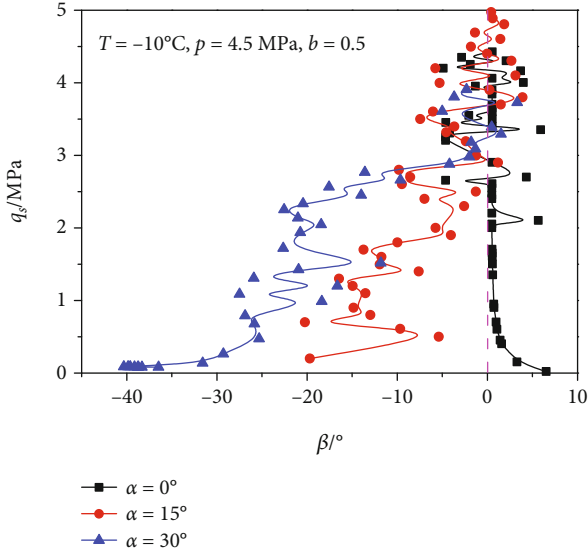


FIGURE 15: Variations of non-coaxial angle with shear stress under different principal stress directions.

presents the variation in the direction of the principal strain increment with q_s . The principal strain increment directions of the FSS and stress path do not coincide at $\alpha = 15^\circ$ and 30° ; however, when $\alpha = 0^\circ$, the non-coaxial behavior of the FSS remains unclear. When $\alpha = 15^\circ$ and 30° , the non-coaxial angle of the FSS (the non-coaxial angle was approximately 20° and 40° in the early stage, respectively) decreases as q_s increases, and the degree of non-coaxiality of the FSS decreases as the hollow cylindrical specimen approaches failure. Initially, the axes of the principal stress and principal strain increment are non-coincident. The non-coaxial angle of the FSS at $\alpha = 30^\circ$ is inferred to be greater than that at $\alpha = 15^\circ$. Namely, for variations in the non-coaxiality of the FSS under different fixed principal stress directions, the non-coaxial angle fluctuation increases as the directional angle of the major principal stress increases.

As illustrated in Figure 16, the stress envelope surface is represented by the $(\sigma_z - \sigma_\theta)/2$ versus the $\tau_{z\theta}$ stress space. Meanwhile, various directions of the principal stress and principal strain increment are presented. According to Equation (1), the angle is formed by $(\sigma_z - \sigma_\theta)/2$ and the stress path is twice the directional angle of the major principal stress. At $\alpha = 15^\circ$, the direction of the principal strain increment of the FSS deviates slightly from that of the principal stress. In tests with $\alpha = 30^\circ$, there are relatively large deviations between the direction of principal stress and principal strain increment.

4.4.2. Non-coaxiality of the FSS under Different Mean Principal Stresses. Figure 17 depicts the non-coaxial behavior of the FSS between the axes of the principal stresses and principal strain increments under different mean principal stresses. The non-coaxiality of the FSS with shear stress follows the same change rule as that of the FSS under $\alpha = 15^\circ$ and 30° . When q_s is small, the non-coaxial angle of the FSS

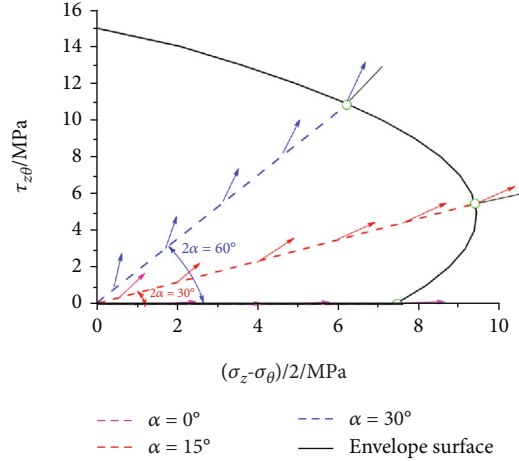


FIGURE 16: Direction of principal strain increment along different principal stress directions.

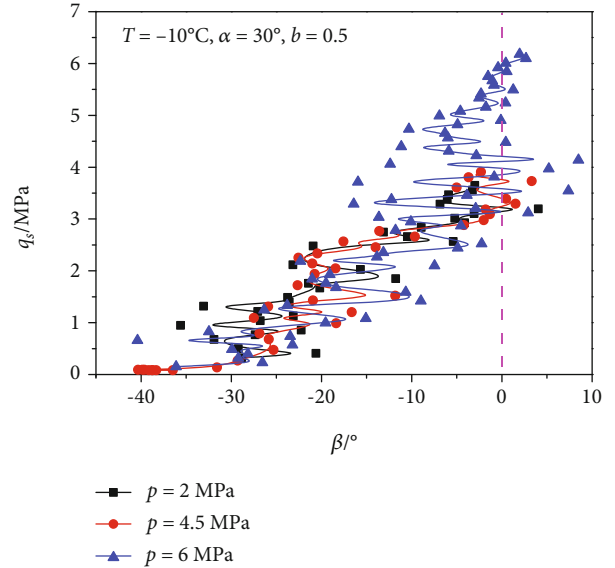


FIGURE 17: Variations of non-coaxial angle with shear stress under mean principal stresses.

is larger, and as q_s increases, the non-coaxial angle of the FSS gradually decreases. When the hollow cylindrical specimen of the FSS is nearing failure, the non-coaxial angle reaches its minimum value, thus indicating that as the shear stress increases, the direction of the principal strain increment and the direction of the principal stress tend to be coaxial. In other words, the deviation of the non-coaxial angle of the FSS can be as large as 35° in the early stage of shearing. Subsequently, the deviation decreases as the shear strain increases, and the non-coaxiality behavior of the FSS is almost coaxiality at failure. The evolution law of the non-coaxial angle of the FSS does not change as the mean principal stress changes and remains within a certain range.

5. Conclusions

A series of hollow cylinder tests of frozen soil were conducted at various directional angles of major principal stress and mean principal stresses, to investigate the anisotropic behavior and non-coaxiality of the FSS under the influence of the principal stress direction. The evolution of the anisotropic behavior and non-coaxiality of the FSS was analyzed under different principal stress directions. Based on this analysis, the following conclusions were drawn:

- (1) The linear variation of the stress components (σ_z , σ_r , σ_θ , and $\tau_{z\theta}$) of the FSS as q_s increases for various directional angles of major principal stress and mean principal stresses. The relationships between shear stress and strain components (ε_z , $\gamma_{z\theta}$, ε_r , and ε_θ) of the FSS with different directional angles of major principal stress and mean principal stresses exhibited a nonlinear increasing trend with a linear increase in shear stress, thus indicating that the growth in the strain components slowed in the early stage and then accelerated near failure.
- (2) The stress-strain-strength anisotropy of frozen soil was determined to be strongly dependent on the principal stress direction. The FSS strength gradually decreased as the directional angle of the major principal stress increased. However, as the mean principal stress increased, the FSS strength decreased. The FSS strength was greater than that of frozen clay under the same directional angle of the major principal stress.
- (3) The non-coaxiality of the FSS was highly dependent on the direction of principal stress. The non-coaxial angle of the FSS increased gradually with an increase in the directional angles of the major principal stress under the directional shear stress path; however, the non-coaxial angle of the FSS did not change with a change in the mean principal stress. The non-coaxial angle of the FSS was observed to be as large as 35° in the early stage of shearing under different mean principal stresses. As the shear stress increased, the direction of the principal strain increment and principal stress tended to become coaxial.

Nomenclature

W :	Axial load (MPa)
M_T :	Torque (N·m)
p_i, p_o :	Inner and outer cell pressure (MPa)
T :	Temperature ($^\circ\text{C}$)
H_o :	Initial specimen height (mm)
Δh :	Axial displacement (mm)
u_i, u_o :	Inner and outer radius displacement (mm)
$\Delta\theta$:	Twist deformation ($^\circ$)
r_i, r_o :	Inner and outer specimen radius (mm)
r_p :	Loading rod radius (mm)
p :	Mean principal stress (MPa)
q :	Deviatoric stress (MPa)

q_s :	Shear stress (MPa)
b :	Coefficient of intermediate principal stress
α :	Directional angle of major principal stress ($^\circ$)
σ_z :	Axial stress (MPa)
$\tau_{z\theta}$:	Circumferential shear stress (MPa)
σ_r :	Radial stress (MPa)
σ_θ :	Circumferential normal stress (MPa)
β :	Non-coaxial angle ($^\circ$)
ε_1 :	Major principal strain (%)
ε_2 :	Intermediate principal strain (%)
ε_3 :	Minor principal strain (%)
α_{ds} :	Direction of principal strain increment
$\gamma_{z\theta}$:	Circumferential shear strain (%)
$d\gamma_{z\theta}$:	Increments of circumferential shear strain
ε_z :	Axial strain (%)
$d\varepsilon_z$:	Increments of axial strain
ε_θ :	Circumferential normal strain (%)
$d\varepsilon_\theta$:	Increments of circumferential normal strain
ε_r :	Radial strain (%)
γ_g :	Generalized shear strain (%)
σ_1 :	Major principal stress (MPa)
σ_2 :	Intermediate principal stress (MPa)
σ_3 :	Minor principal stress (MPa)

Acronyms

HCA:	Hollow cylinder apparatus
FHCA-300:	Dynamic hollow cylinder apparatus for frozen soil
FSS:	Frozen standard sand.

Data Availability

The authors claim that the data used to support the findings of this study are available from the corresponding author upon request.

Conflicts of Interest

The authors declare that they have no conflicts of interest.

Acknowledgments

This study was supported by the China's Second Tibetan Plateau Scientific Expedition and Research (2019QZKK0905), the State Key Laboratory for Geomechanics and Deep Underground Engineering, the China University of Mining and Technology (SKLGDUEK1904), and the Research Project of the State Key Laboratory of Frozen Soils Engineering (Grant No. SKLFSE-ZY-20, SKLFSE-ZQ-58).

References

- [1] M. J. Symes, A. Gens, and D. W. Hight, "Undrained anisotropy and principal stress rotation in saturated sand," *Geotechnique*, vol. 34, no. 1, pp. 11–27, 1984.
- [2] B. L. Zhang, D. Y. Wang, Z. W. Zhou, W. Ma, and L. L. Lei, "The effect of temperature on dynamic characteristics of frozen clay under principal stress rotation," *Advances in*

- Materials Science and Engineering*, vol. 2021, Article ID 3127253, 16 pages, 2021.
- [3] M. Y. Fattah, "Effect of initial stress anisotropy on the cyclic behaviour of sand," *Engineering and Technology Journal*, vol. 24, no. 5, pp. 472–498, 2005.
 - [4] M. Y. Fattah, R. R. Al-Omari, and M. K. Hameedi, "Tracing of stresses and pore water pressure changes during a multistage modified relaxation test model on organic soil," *Arabian Journal of Geosciences*, vol. 14, no. 19, p. 1976, 2021.
 - [5] K. A. Klein and J. C. Santamarina, "Electrical conductivity in soils: underlying phenomena," *Journal of Environmental and Engineering Geophysics*, vol. 8, no. 4, pp. 263–273, 2003.
 - [6] W. M. Ye, L. D. Yang, Y. Huang, Y. Q. Tang, and B. Y. Dong, "Anisotropy characteristics of micro voids in Shanghai soft soil and its cause analysis," *Journal of Engineering Geology*, vol. 12, pp. 84–87, 2004.
 - [7] M. J. Jiang, C. Fu, J. D. Liu, and T. Li, "Discrete element analysis of anisotropic structured sand," *Rock and Soil Mechanics*, vol. S1, pp. 577–584, 2015.
 - [8] S. R. Bodner, "A hardness law for inelastic deformation," *International Journal of Engineering Science*, vol. 16, no. 3, pp. 221–230, 1978.
 - [9] X. N. Gong, "Preliminary discussion on anisotropy of soft clay foundation," *Journal of Zhejiang University*, vol. 4, pp. 103–115, 1986.
 - [10] J. R. F. Authur and B. K. Menzies, "Inherent anisotropy in a sand," *Geotechnique*, vol. 22, no. 1, pp. 115–128, 1972.
 - [11] P. V. Lade and J. M. Duncan, "Closure to "Cubical triaxial tests on cohesionless Soil"," *Journal of Geotechnical and Geoenvironmental Engineering*, vol. 101, no. 5, pp. 491–493, 1975.
 - [12] S. Nishimura, R. J. Jardine, and N. A. Minh, "Shear strength anisotropy of natural London clay," *Géotechnique*, vol. 57, no. 1, pp. 49–62, 2007.
 - [13] Y. Shen, *Experimental Study on Undisturbed Soft Clay Considering the Change of Principal Stress Direction*, Zhejiang University, Hangzhou, 2007.
 - [14] Z. X. Yang, X. Y. Li, and H. Y. Ming, "Study on anisotropy and undrained shear properties of sand," *Journal of Shenzhen University: Science and Technology Edition*, vol. 26, no. 2, pp. 158–163, 2009.
 - [15] Y. L. Yu, J. M. Zhang, C. X. Tong, and G. Zhang, "Mechanical response of anisotropic sand in axial drained shear test," *Rock and Soil Mechanics*, vol. 32, no. 6, pp. 1637–1642, 2011.
 - [16] H. R. Razeghi and H. M. Romiani, "Experimental investigation on the inherent and initial induced anisotropy of sand," *KSCE Journal of Civil Engineering*, vol. 19, no. 3, pp. 583–591, 2015.
 - [17] H. Xiong, L. Guo, Y. Cai, and Z. Yang, "Experimental study of drained anisotropy of granular soils involving rotation of principal stress direction," *European Journal of Environmental and Civil Engineering*, vol. 20, no. 4, pp. 431–454, 2016.
 - [18] J. Zhou, J. J. Yan, Z. Y. Liu, and X. N. Gong, "Undrained anisotropy and non-coaxial behavior of clayey soil under principal stress rotation," *Journal of Zhejiang University*, vol. 15, no. 4, pp. 241–254, 2014.
 - [19] J. G. Qian, Z. B. Du, and Z. Y. Yin, "Cyclic degradation and non-coaxiality of soft clay subjected to pure rotation of principal stress directions," *Acta Geotechnica*, vol. 13, no. 4, pp. 943–959, 2018.
 - [20] Y. Y. Cai, *An Experimental Study of Non-coaxial Soil Behavior Using Hollow Cylinder Testing*, University of Nottingham, Nottingham, 2010.
 - [21] K. H. Roscoe, R. H. Bassett, and E. R. L. Cole, "Principal axes observed during simple shear of a sand," in *Proceedings of the 4th European Conference on Soil Mechanics and Foundation Engineering*, pp. 231–237, Norwegian Geotechnical Institute, 1967.
 - [22] R. K. S. Wong and J. R. F. Arthur, "Sand sheared by stresses with cyclic variations in direction," *Géotechnique*, vol. 36, no. 2, pp. 215–226, 1986.
 - [23] K. Ishihara and I. Towhata, "Sand response to cyclic rotation of principal stress directions as induced by wave loads," *Soils and Foundations*, vol. 23, no. 4, pp. 11–26, 1983.
 - [24] K. Mirua, S. Miura, and S. Toki, "Deformation behavior of anisotropic dense sand under principal stress axes rotation," *Soils and Foundations*, vol. 26, no. 1, pp. 36–52, 1986.
 - [25] D. Pradel, K. Ishihara, and M. Gutierrez, "Yielding and flow of sand under principal stress axes rotation," *Soils and Foundations*, vol. 30, no. 1, pp. 87–99, 1990.
 - [26] M. Gutierrez, K. Ishihara, and I. Towhata, "Flow theory for sand during rotation of principal stress direction," *Soils and Foundations*, vol. 31, no. 4, pp. 121–132, 1991.
 - [27] P. V. Lade and M. M. Kirkgard, "Effects of stress rotation and changes of B-values on cross-anisotropic behavior of natural, K0-consolidated soft clay," *Soils and Foundations*, vol. 40, no. 6, pp. 93–105, 2000.
 - [28] Y. Y. Cai, H. S. Yu, D. Wanatowski, and X. Li, "Noncoaxial behavior of sand under various stress paths," *Journal of Geotechnical and Geoenvironmental Engineering*, vol. 139, no. 8, pp. 1381–1395, 2012.
 - [29] J. J. Yan, J. Zhou, X. N. Gong, and Y. Cao, "Undrained response of reconstituted clay to cyclic pure principal stress rotation," *Journal of Central South University*, vol. 22, no. 1, pp. 280–289, 2015.
 - [30] Y. M. Yang, W. B. Fei, H. S. Yu, J. Ooi, and M. Rotter, "Experimental study of anisotropy and non-coaxiality of granular solids," *Granular Matter*, vol. 17, no. 2, pp. 189–196, 2015.
 - [31] V. R. Parameswaran, "Deformation behaviour and strength of frozen sand," *Canadian Geotechnical Journal*, vol. 17, no. 1, pp. 74–88, 1980.
 - [32] Y. L. Zhu and D. L. Carbee, "Uniaxial compressive strength of frozen silt under constant deformation rates," *Cold Regions Science and Technology*, vol. 9, no. 1, pp. 3–15, 1984.
 - [33] M. Christ and J. B. Park, "Laboratory determination of strength properties of frozen rubber-sand mixtures," *Cold Regions Science and Technology*, vol. 60, no. 2, pp. 169–175, 2010.
 - [34] X. T. Xu, Y. B. Wang, Z. H. Yin, and H. W. Zhang, "Effect of temperature and strain rate on mechanical characteristics and constitutive model of frozen Helin loess," *Cold Regions Science and Technology*, vol. 136, pp. 44–51, 2017.
 - [35] M. D. Shen, Z. W. Zhou, and S. J. Zhang, "Effect of stress path on mechanical behaviours of frozen subgrade soil," *Road Materials and Pavement Design*, vol. 8, pp. 1–30, 2021.
 - [36] Z. W. Zhou, W. Ma, S. J. Zhang, Y. Mu, and G. Li, "Experimental investigation of the path-dependent strength and deformation behaviours of frozen loess," *Engineering Geology*, vol. 265, article 105449, 2020.
 - [37] Z. W. Zhou, G. Y. Li, M. D. Shen, and Q. Wang, "Dynamic responses of frozen subgrade soil exposed to freeze-thaw cycles," *Soil Dynamics and Earthquake Engineering*, vol. 152, p. 107010, 2022.
 - [38] D. Chen, D. Y. Wang, W. Ma, L. Lei, and G. Li, "A strength criterion for frozen clay considering the influence of stress Lode

- angle,” *Canadian Geotechnical Journal*, vol. 56, no. 11, pp. 1557–1572, 2019.
- [39] D. Chen, W. Ma, G. Y. Li, Z. Zhou, and Y. Mu, “A long-term strength criterion for frozen clay under complex stress states,” *Cold Regions Science and Technology*, vol. 176, p. 103089, 2020.
- [40] L. Zdravkovic, D. M. Potts, and D. W. Hight, “The effect of strength anisotropy on the behaviour of embankments on soft ground,” *Géotechnique*, vol. 52, no. 6, pp. 447–457, 2002.
- [41] D. Chen, W. Ma, G. Y. Li, Z. Zhou, Y. Mu, and S. Chen, “Definition of failure criterion for frozen soil under directional shear-stress path,” *Sciences in Cold and Arid Regions*, vol. 11, no. 6, pp. 428–434, 2019.
- [42] D. W. Hight, A. Gens, and M. J. Symes, “The development of a new hollow cylinder apparatus for investigating the effects of principal stress rotation in soils,” *Géotechnique*, vol. 33, no. 4, pp. 355–383, 1983.